Optimal Attitude Control for a Rigid Body with Symmetry

Taeyoung Lee*†, N. Harris McClamroch†
Department of Aerospace Engineering
University of Michigan, Ann Arbor, MI 48109
{tylee, nhm}@umich.edu

Melvin Leok*
Department of Mathematics
Purdue University, West Lafayette, IN 47907
mleok@math.purdue.edu

***Abstract*— Optimal control problems are formulated and efficient computational procedures are proposed for attitude dynamics of a rigid body with symmetry. The rigid body is assumed to act under a gravitational potential and under a structured control moment that respects the symmetry. The symmetry in the attitude dynamics system yields a conserved quantity, and it causes a fundamental singularity in the optimal control problem. The key feature of this paper is its use of computational procedures that are guaranteed to avoid the numerical ill-conditioning that originates from this symmetry. It also preserves the geometry of the attitude dynamics. The theoretical basis for the computational procedures is summarized, and examples of optimal attitude maneuvers for a 3D pendulum are presented.**

I. Introduction

We study a discrete optimal control problem for attitude dynamics of a rigid body with symmetry. The attitude is represented by a rotation matrix, which has a Lie group structure denoted by $\mathrm{SO}(3)$. We assume that the rigid body is acting under an attitude dependent potential, and the potential is invariant under a symmetry action. The external control input is formulated such that it respects the symmetry. This problem provides both a theoretical challenge and a numerical challenge in the sense that the configuration space has a Lie group structure, and the conserved quantity causes ill-conditioning of the numerical optimization.

General purpose numerical integration methods, including the popular Runge-Kutta schemes, typically preserve neither the group structure of the attitude configuration space nor the invariant properties of the dynamics. Geometric structure-preserving integrators are symplectic and momentum preserving, and they exhibit good energy behavior for an exponentially long time period [1]. In particular, Lie group variational integrators have the desirable properties that they preserve the group structure as well as the geometric features, without needs of local parameterization, reprojection, or constraints [2], [3]. The exact geometric properties of the discrete flow not only generate improved qualitative behavior, but also allow for accurate long-time simulation.

Optimal control problems on a Lie group have been studied in [4], [5], [6]. These studies are based on the driftless kinematics of a Lie group. The dynamics are ignored, and elements in the corresponding Lie algebra are considered as control inputs. The discrete optimal control problems of a rigid body are studied in [7], [8], where the dynamics as well as the kinematics equations are explicitly utilized, and an efficient numerical algorithm to solve discrete optimality conditions is presented.

This paper introduces geometrically exact and numerically efficient computational approaches to solve the optimal control problems of the attitude dynamics of a rigid body with symmetry and structured control input. The dynamics are discretized by a Lie group variational integrator, and discrete necessary conditions for optimality are constructed. The utilization of the Lie group variational integrator is justified in this problem, since it preserves the momentum map originating from the symmetry. The rigid body is underactuated since the control input does not act along the symmetry direction. The symmetry of the controlled dynamics causes difficulties in solving the necessary conditions for optimality. A simple numerical approach is presented to overcome this numerical ill-conditioning.

This paper is organized as follows. In Section II, a 3D pendulum is presented as a model of rigid body attitude dynamics, and the symmetry of the 3D pendulum is described. An optimal control problem with symmetry is studied in Section III, and numerical results are given in Section IV.

II. Dynamics of a 3D Pendulum

A 3D pendulum is a rigid body supported by a fixed frictionless pivot acting under the influence of uniform gravitational field [9]. We use a 3D pendulum model to study the optimal control for attitude dynamics of a rigid body, since it has three degrees of rotational freedom, and the gravitational potential has a symmetry: it is invariant under a rotation about the gravity direction.

In this section, the continuous equations of motion are presented. The symmetry of the 3D pendulum are discussed, and the control input structure is described. Discrete equations of motion, referred to as a Lie group variational integrator, are described for a controlled 3D pendulum model.

A. Continuous equations of motion

The configuration space of the 3D pendulum is $\mathrm{SO}(3)$. We identify the tangent bundle $\mathrm{TSO}(3)$ with $\mathrm{SO}(3)\times\mathfrak{so}(3)$ by left translation, and we identify $\mathfrak{so}(3)$ with $\mathbb{R}^3$ by an isomorphism $S(\cdot):\mathbb{R}^3\mapsto\mathfrak{so}(3)$ defined by the condition that $S(x)y=x\times y$ for any $x,y\in\mathbb{R}^3$. We denote the attitude and the angular velocity of the rigid body as $(R,\Omega)\in \mathrm{T}_R\mathrm{SO}(3)$. The rotation matrix $R\in\mathrm{SO}(3)$ transforms a

*This research has been supported in part by NSF under grant DMS-0504747, and by a grant from the Rackham Graduate School, University of Michigan.

†This research has been supported in part by NSF under grant ECS-0244977.

vector represented in the body fixed frame to one represented in the inertial frame.

Let $\rho \in \mathbb{R}^3$ be a vector from the pivot point to the mass center of the rigid body expressed in the body fixed frame, and let $m, g \in \mathbb{R}$ and $J \in \mathbb{R}^{3\times3}$ be the mass of the rigid body, the gravitational acceleration, and the moment of inertia matrix of the rigid body about the pivot point, respectively. The Lagrangian of the 3D pendulum $L : \mathrm{TSO}(3) \mapsto \mathbb{R}$ is given by

$$L(R,\Omega) = \frac{1}{2}\mathrm{tr}\big[S(\Omega)J_d S(\Omega)^T\big] + mge_3^T R\rho,$$

where $J_d \in \mathbb{R}^{3\times3}$ is a nonstandard moment of inertia defined by $J_d = \frac{1}{2}\mathrm{tr}[J]\, I_{3\times3} - J$, and we set the gravitational direction in the inertial frame as $e_3 = [0;0;1] \in \mathbb{S}^2$.

The continuous equations, derived from the Lagrange-d'Alembert principle, are given by

$$\dot{\Pi} + \Omega \times \Pi = mg\rho \times R^T e_3 + M, \tag{1}$$

$$\dot{R} = RS(\Omega), \tag{2}$$

where $\Pi = J\Omega \in \mathbb{R}^3$ is the angular momentum in the body fixed frame, and $M \in \mathbb{R}^3$ is the external control moment.

B. Symmetry of 3D pendulum

The kinetic energy of the rigid body is left invariant on $\mathrm{TSO}(3)$, and the gravitational potential energy is invariant under a rotation about the gravity direction, which can be represented by the left action of the subgroup $\big\{\exp S(\theta e_3) \in \mathrm{SO}(3)\big|\theta \in \mathbb{S}^1\big\}$.

As a result, the Lagrangian of the 3D pendulum has a symmetry action by $\mathbb{S}^1$, $\Phi_\theta : \mathbb{S}^1 \times \mathrm{SO}(3) \mapsto \mathrm{SO}(3)$ given by

$$\Phi_\theta(R) = \exp S(\theta e_3)\, R,$$

for $\theta \in \mathbb{S}^1$. It can be shown that $\Phi_\theta^* L(R,\Omega) = L(R,\Omega)$.

Suppose that there is no external control input. Noether's theorem states that a symmetry in the Lagrangian yields conservation of the momentum map. For the 3D pendulum, the momentum map of the symmetry action Φ_θ corresponds to the inertial angular momentum of the rigid body about the gravity direction $\pi_3 = e_3^T RJ\Omega \in \mathbb{R}$. It is conserved for the free dynamics of the 3D pendulum.

The structure of the control input respects the symmetry of the uncontrolled free dynamics of the 3D pendulum, namely

$$M = R^T e_3 \times u,$$

for a control parameter $u \in \mathbb{R}^3$. Since the external control moment has no component along the gravity direction, the angular momentum about the gravity direction is also preserved in the controlled dynamics. Such control inputs are physically utilized by actuation mechanisms, such as point mass actuators, that change the center of mass of the 3D pendulum.

Here we introduce the concept of a geometric phase, and it is used to interpret the numerical optimization result in Section IV. Using the symmetry, the dynamics of the 3D pendulum can be expressed in terms of $\Gamma = R^T e_3$ in the reduced configuration space $\mathrm{SO}(3)/\mathbb{S}^1 \simeq \mathbb{S}^2$. The corresponding flow in the original configuration space is reconstructed by lifting to a level set of the conserved quantity. Suppose that the trajectory in the reduced space is a closed loop, i.e. $\Gamma(0) = \Gamma(T)$ for some $T > 0$, and the value of the angular momentum about the gravity direction is zero. Then, the terminal attitude is related to the initial attitude by a symmetric action. More explicitly, we have

$$R(T) = \Phi_{\theta_{\text{geo}}}(R(0)),$$

where θ_{geo} is the geometric phase determined by

$$\theta_{\text{geo}} = \int_{\mathcal{B}} \frac{2\,\|J\Gamma\|^2 - \mathrm{tr}[J]\,(\Gamma^T J\Gamma)}{(\Gamma^T J\Gamma)^2}\, dA, \tag{3}$$

where $\mathcal{B}$ is a surface in $\mathbb{S}^2$ whose boundary is $\big\{\Gamma(t)\big|t \in [0,T]\big\}$ [10]. Note that the geometric phase is determined only by the reduced trajectory of Γ and the characteristics of the rigid body J. It is independent of the velocity $\dot{\Gamma}$.

C. Lie group variational integrator

The attitude of the 3D pendulum is represented by a rotation matrix $R \in \mathrm{SO}(3)$. The conserved quantity, arising from symmetry, is emphasized in this study. However, the most common numerical integration methods, including the widely used Runge-Kutta schemes, neither preserve the Lie group structure nor first integrals. In addition, standard Runge-Kutta methods fail to capture the energy dissipation of a controlled system accurately [11]. For example, if we integrate (2) by a typical Runge-Kutta scheme, the quantity $R^T R$ inevitably drifts from the identity matrix as the simulation time increases. It is often proposed to parameterize (2) by Euler angles or unit quaternions. However, Euler angles are not global expressions of the attitude since they have associated singularities. Unit quaternions do not exhibit singularities, but are constrained to lie on the unit three-sphere $\mathbb{S}^3$, and general numerical integration methods do not preserve the unit length constraint. Therefore, quaternions have the same numerical drift problem. Renormalizing the quaternion vector at each step tends to break other conservation properties. Furthermore, unit quaternions, which are diffeomorphic to $\mathrm{SU}(2)$, double cover $\mathrm{SO}(3)$. So there are inevitable ambiguities in expressing the attitude using quaternions.

In [2], Lie group variational integrators are introduced by explicitly adopting the approach of Lie group methods [12] to the discrete variational principle [11]. They have the desirable property that they are symplectic and momentum preserving, and they exhibit good energy behavior for an exponentially long time period. They also preserve the Lie group structure without the use of local charts, reprojection, or constraints.

Using the results in [2], a Lie group variational integrator on $\mathrm{SO}(3)$ is given for the 3D pendulum by

$$hS(\Pi_k) = F_k J_d - J_d F_k^T, \tag{4}$$

$$R_{k+1} = R_k F_k, \tag{5}$$

$$\Pi_{k+1} = F_k^T \Pi_k + hmg\rho \times R_{k+1}^T e_3 + hR_{k+1}^T e_3 \times u_{k+1}, \tag{6}$$

where the subscript k denotes the kth discrete variable for a fixed integration step size $h \in \mathbb{R}$, and $F_k \in \mathrm{SO}(3)$ is the relative attitude between two adjacent integration steps. For a given (R_k, Π_k) and control inputs, (4) is solved to find F_k. Then (R_{k+1}, Π_{k+1}) is obtained by (5) and (6). This yields a map $(R_k, \Pi_k) \mapsto (R_{k+1}, \Pi_{k+1})$ and this process is repeated. The only implicit part is (4). The actual computation of F_k is done in the Lie algebra $\mathfrak{so}(3)$ of dimension 3, and the rotation matrices are updated by multiplication. So this approach is distinguished from integration of the kinematics equation (2), and there is no excessive computational burden. The properties of these discrete equations of motion are discussed more explicitly in [2], [3]. We use these discrete equations of motion to formulate the following optimal control problem.

III. Optimal control with symmetry

We formulate an optimal attitude control problem for a 3D pendulum with symmetry. Necessary conditions for optimality are developed and computational approaches are presented to solve the corresponding two point boundary value problem.

A. Problem formulation

A discrete time optimal control problem is formulated as a maneuver of the rigid pendulum body from a given initial attitude $R_0 \in \mathrm{SO}(3)$ and an initial angular momentum $\Pi_0 \in \mathbb{R}^3$ to a desired terminal attitude $R_N^d \in \mathrm{SO}(3)$ and a terminal angular momentum $\Pi_N^d \in \mathbb{R}^3$ during a given maneuver time N. The performance index is the square of the l_2 norm of the control inputs:

$$\begin{gathered}\text{given: } (R_0, \Pi_0),\ (R_N^d, \Pi_N^d),\ N,\\ \min_{u_{k+1}} \mathcal{J} = \sum_{k=0}^{N-1} \frac{h}{2} \left\| u_{k+1} \right\|^2,\\ \text{such that } R_N = R_N^d,\ \Pi_N = \Pi_N^d,\\ \text{subject to (4), (5) and (6).}\end{gathered}$$

B. Necessary conditions of optimality

Variational models: The necessary conditions of optimality are developed using the standard variational approach. We first derive certain variational formulas. The variation of $R_k \in \mathrm{SO}(3)$ can be expressed in terms of a Lie algebra element $S(\zeta_k) \in \mathfrak{so}(3)$ for $\zeta_k \in \mathbb{R}^3$ and the exponential map as

$$R_k^\epsilon = R_k \exp \epsilon S(\zeta_k).$$

The corresponding infinitesimal variation is given by

$$\delta R_k = \left. \frac{d}{d\epsilon} \right|_{\epsilon=0} R_k \exp \epsilon S(\zeta_k) = R_k S(\zeta_k). \tag{7}$$

This gives an expression for the infinitesimal variation of a Lie group element in terms of its Lie algebra. Then, small perturbations from a given trajectory can be written as

$$\Pi_k^\epsilon = \Pi_k + \epsilon \delta \Pi_k, \tag{8}$$

$$R_k^\epsilon = R_k + \epsilon R_k S(\zeta_k) + \mathcal{O}(\epsilon^2), \tag{9}$$

where $\delta\Pi_k, \zeta_k$ are considered as elements of $\mathbb{R}^3$.

We derive expressions for the constrained variation of F_k using its definition (5) and the variation of the rotation matrix (9). Since $F_k = R_k^T R_{k+1}$, the infinitesimal variation δF_k is given by

$$\begin{aligned}\delta F_k &= \delta R_k^T R_{k+1} + R_k^T \delta R_{k+1},\\ &= -S(\zeta_k) F_k + F_k S(\zeta_{k+1}).\end{aligned}$$

We can also write $\delta F_k = F_k S(\xi_k)$ for $\xi_k \in \mathbb{R}^3$ using (7). Using the property $S(R^T x) = R^T S(x) R$ for any $R \in \mathrm{SO}(3)$ and $x \in \mathbb{R}^3$, we obtain the constrained variation of F_k as

$$\xi_k = -F_k^T \zeta_k + \zeta_{k+1}. \tag{10}$$

We now relate the constrained variation of $\delta\Pi_k$ to ξ_k by starting with (4). Taking a variation of (4), we obtain

$$hS(\delta\Pi_k) = F_k S(\xi_k) J_d + J_d S(\xi_k) F_k^T.$$

Using the properties, $S(Rx) = RS(x)R^T$ and $S(x)A + A^T S(x) = S(\{\mathrm{tr}[A]\, I_{3\times 3} - A\}\, x)$ for any $x \in \mathbb{R}^3$, $A \in \mathbb{R}^{3\times 3}$, and $R \in \mathrm{SO}(3)$, the above equation is rewritten as

$$hS(\delta\Pi_k) = S(\{\mathrm{tr}[F_k J_d]\, I_{3\times 3} - F_k J_d\}\, F_k \xi_k).$$

Thus, ξ_k is given by

$$\xi_k = hF_k^T \left\{\mathrm{tr}[F_k J_d]\, I_{3\times 3} - F_k J_d\right\}^{-1} = \mathcal{B}_k \delta\Pi_k, \tag{11}$$

where $\mathcal{B} \in \mathbb{R}^{3\times 3}$.

Necessary conditions: Define an augmented performance index as

$$\begin{aligned}\mathcal{J}_a = \sum_{k=0}^{N-1} \frac{h}{2} \left\| u_{k+1} \right\|^2 &+ \lambda_k^{1,T} S^{-1}\big(\mathrm{logm}(F_k - R_k^T R_{k+1})\big)\\ &+ \lambda_k^{2,T} \left\{-\Pi_{k+1} + F_k^T \Pi_k + hmg\rho \times R_{k+1}^T e_3\right\}\\ &+ \lambda_k^{2,T} \left\{R_{k+1}^T e_3 \times u_{k+1}\right\},\end{aligned} \tag{12}$$

where $\lambda_k^1, \lambda_k^2 \in \mathbb{R}^3$, are Lagrange multipliers corresponding to the discrete equations of motion (5) and (6). The constraint (4) is applied implicitly by (11) when taking the variation.

Using the variational models (8)–(11), and the fact that the variations ζ_k, $\delta\Pi_k$ vanish at $k = 0, N$, the infinitesimal variation of the augmented performance index is written as

$$\begin{aligned}\delta\mathcal{J}_a = \sum_{k=1}^{N-1} &h\delta u_k^T \left\{u_k - R_k^T e_3 \times \lambda_{k-1}^2\right\}\\ &+ \zeta_k^T \left\{-\lambda_{k-1}^1 + \mathcal{A}_k^T \lambda_k^1 + \mathcal{C}_k^T \lambda_k^2 - hF_k u_{k+1} e_3^T R_{k+1}\right\}\\ &+ \delta\Pi_k^T \left\{-\lambda_{k-1}^2 + \mathcal{B}_k^T \lambda_k^1 + \mathcal{D}_k^T \lambda_k^2 - h\mathcal{B}_k^T u_{k+1} e_3^T R_{k+1}\right\},\end{aligned}$$

where

$$\begin{aligned}\mathcal{A}_k &= F_k^T,\\ \mathcal{B}_k &= hF_k^T \left\{\mathrm{tr}[F_k J_d]\, I_{3\times 3} - F_k J_d\right\}^{-1},\\ \mathcal{C}_k &= hmgS(\rho) S(R_{k+1}^T e_3) F_k^T,\\ \mathcal{D}_k &= F_k^T + S(F_k^T \Pi_k)\mathcal{B}_k + hmgS(\rho) S(R_{k+1}^T e_3)\mathcal{B}_k.\end{aligned}$$

Since $\delta \mathcal{J}_a = 0$ for all variations of $\delta u_k, \zeta_k, \delta \Pi_k$, the expressions in the braces of the above equation are zero. Thus we obtain necessary conditions for optimality as follows.

$$hS(\Pi_k) = F_k J_d - J_d F_k^T, \tag{13}$$

$$R_{k+1} = R_k F_k, \tag{14}$$

$$\Pi_{k+1} = F_k^T \Pi_k + hmg\rho \times R_{k+1}^T e_3 + hR_{k+1}^T e_3 \times u_{k+1}, \tag{15}$$

$$u_{k+1} = R_{k+1}^T e_3 \times \lambda_k^2, \tag{16}$$

$$\begin{bmatrix} \lambda_k^1 \\ \lambda_k^2 \end{bmatrix} = \begin{bmatrix} \mathcal{A}_{k+1}^T & \mathcal{C}_{k+1}^T - hF_{k+1} u_{k+2} e_3^T R_{k+2} \\ \mathcal{B}_{k+1}^T & \mathcal{D}_{k+1}^T - h\mathcal{B}_{k+1}^T u_{k+2} e_3^T R_{k+2} \end{bmatrix} \begin{bmatrix} \lambda_{k+1}^1 \\ \lambda_{k+1}^2 \end{bmatrix}. \tag{17}$$

In the above equations, the implicit parts are (13) and (17). For a given initial condition $(R_0, \Pi_0, \lambda_0^1, \lambda_0^2)$, we can find F_0 by solving (13). Then, R_1 is obtained by (14). Since $u_1 = R_1^T e_3 \times \lambda_0^2$ by (16), Π_1 can be obtained using (15). We solve (13) to obtain F_1 using Π_1. Finally, λ_1^1, λ_1^2 are obtained by solving the implicit equation (17), since $\mathcal{A}_1, \mathcal{B}_1, \mathcal{C}_1, \mathcal{D}_1$ are functions of R_1, Π_1, F_1.

The implicit equation (13) is solved by Netwon's iteration in the Lie algebra, and the implicit equation (17) is solved by fixed point iteration. Numerical computations show that two or three iterations are typically required to achieve machine precision.

C. Two point boundary value problem

The necessary conditions for optimality are given by a 12 dimensional two point boundary value problem. This problem is to find the optimal discrete flow, multipliers, and control inputs to satisfy the equations of motion (13)–(15), optimality condition (16), multiplier equations (17), and boundary conditions simultaneously.

We substitute the optimality condition (16) into the equations of motion and the multiplier equations, and we apply the shooting method to solve the two point boundary value problem using sensitivity derivatives. The shooting method is numerically efficient in the sense that the number of iteration parameters is minimized; 6 elements of the initial Lagrange multiplier are iterated. In other approaches, the entire discrete trajectory of the control input and Lagrange multiplier are updated.

The drawback of the shooting method is that the extremal solutions are sensitive to small changes in the unspecified initial multiplier values. The nonlinearity makes it hard to construct an accurate estimate of sensitivity. In addition this problem, the symmetry and the underactuation induce numerical ill-conditioning. Therefore, in order to apply the shooting method, it is important to compute the sensitivities accurately, and the effects of the symmetry should be taken into account.

In this paper, the attitude dynamics of a rigid body is described by the structure-preserving Lie group variational integrator, and the sensitivity is expressed in terms of a Lie algebra element. This approach completely avoids any singularity in the attitude representation, and the discrete flow respects the geometric features. The resulting sensitivity derivatives are sufficiently accurate for the shooting method. Furthermore, a simple numerical approach is presented to eliminate the ill-conditioning caused by the symmetry.

Sensitivity derivatives: Taking a variation of the discrete equations of motion and the multiplier equation using the variational models, the linearized equations of motion and the linearized multiplier equations can be written as

$$\begin{aligned} x_{k+1} &= A_k^{11} x_k + A_k^{12} \delta\lambda_k, \\ \delta\lambda_k &= A_{k+1}^{21} x_{k+1} + \left(A_{k+1}^{11}\right)^T \delta\lambda_{k+1}, \end{aligned}$$

where $x_k = [\zeta_k; \delta\Pi_k] \in \mathbb{R}^6$, and matrices $A^{ij} \in \mathbb{R}^{6\times 6}$ are suitably defined. The solution of the linear equations is given by

$$\begin{bmatrix} x_N \\ \delta\lambda_N \end{bmatrix} = \begin{bmatrix} \Psi^{11} & \Psi^{12} \\ \Psi^{21} & \Psi^{22} \end{bmatrix} \begin{bmatrix} x_0 \\ \delta\lambda_0 \end{bmatrix},$$

where $\Psi^{ij} \in \mathbb{R}^{6\times 6}$. For the given two point boundary value problem, the initial attitude and the initial angular momentum are fixed, and the terminal multiplier is free. Thus, we have the following sensitivity equation for the terminal attitude and the terminal angular momentum with respect to the initial multiplier;

$$x_N = \Psi^{12} \delta\lambda_0. \tag{18}$$

Avoiding numerical ill-conditioning: The symmetry yields a conserved quantity by Noether's theorem, and it causes a fundamental singularity in the sensitivity derivatives for the two point boundary value problem. At each iteration, we require the inverse of the sensitivity derivative represented by the matrix Ψ^{12} to update the initial multiplier to satisfy the terminal boundary condition. However, this sensitivity matrix has a theoretical rank deficiency of one since the vertical component of the inertial angular momentum is conserved regardless of the initial multiplier variation. Therefore, equation (18) is numerically ill-conditioned.

Here we presents a simple numerical scheme to avoid the numerical ill-conditioning caused by the symmetry. We decompose the sensitivity derivative into symmetric parts and asymmetric parts. Equation (18) is rewritten as

$$\begin{bmatrix} \zeta_N \\ \delta\Pi_N \end{bmatrix} = \begin{bmatrix} \Psi_1 & \Psi_2 \\ \Psi_3 & \Psi_4 \end{bmatrix} \begin{bmatrix} \delta\lambda_0^1 \\ \delta\lambda_0^2 \end{bmatrix}, \tag{19}$$

where $\Psi_i \in \mathbb{R}^{3\times 3}$ are submatrices of Ψ^{12}. Using the above equation and (7), the infinitesimal variation of the inertial angular momentum is given by

$$\begin{aligned} \delta\pi_N &= \delta(R_N \Pi_N) = \delta R_N \Pi_N + R_N \delta\Pi_N, \\ &= -R_N S(\Pi_N)\zeta_N + R_N \delta\Pi_N, \\ &= -R_N S(\Pi_N)(\Psi_1\lambda_0^1 + \Psi_2\lambda_0^2) + R_N(\Psi_3\lambda_0^1 + \Psi_4\lambda_0^2). \end{aligned}$$

Now, the sensitivity derivative equation (19) can be rewritten in terms of the inertial angular momentum variation as

$$\begin{bmatrix} \zeta_N \\ \delta\pi_N \end{bmatrix} = \begin{bmatrix} \Psi_1 & \Psi_2 \\ R_N(\Psi_3 - S(\Pi_N)\Psi_1) & R_N(\Psi_4 - S(\Pi_N)\Psi_2) \end{bmatrix} \begin{bmatrix} \delta\lambda_0^1 \\ \delta\lambda_0^2 \end{bmatrix}. \tag{20}$$

From the symmetry, the third component of the inertial angular momentum variation is zero; $\delta(\pi_N)_3 = 0$. Thus, the sixth row of the above matrix is zero. (Numerical simulation in the later section shows that the norm of the last row of the transformed sensitivity matrix is at the level of 10^{-15}.) Now, we find an update of the initial multiplier by the pseudo-inverse of the 5×6 matrix;

$$\delta\lambda_0 = \Xi^\dagger x'_N = \Xi^T(\Xi\Xi^T)^{-1}x'_N, \tag{21}$$

where $\Xi \in \mathbb{R}^{5\times 6}$ is composed of the first five rows of the transformed sensitivity derivative in (20), and $x'_N = [\zeta_N; \delta(\pi_N)_1; \delta(\pi_N)_2] \in \mathbb{R}^5$. This approach removes the singularity in the sensitivity derivatives completely, and the resulting optimal control problem is no longer ill-conditioned. Numerical simulations show that the numerical optimization procedure fails without this modification.

Newton iteration: Using the decomposed sensitivity, an initial guess of the unspecified initial conditions is iterated to satisfy the specified terminal boundary conditions in the limit. Any type of Newton iteration can be applied. We use a line search with backtracking algorithm, referred to as Newton-Armijo iteration [13]. The procedure is summarized as follows.

```
Guess an initial multiplier λ_0.
Find Π_k, R_k, λ_k^1, λ_k^2 using (13)–(17).
Compute the terminal B.C. error; Error = ‖x'_N‖.
Set Error^t = Error,  i = 1.
while Error > ε_S.
    Find a line search direction; D = Ξ^†.
    Set c = 1.
    while Error^t > (1 − 2αc)Error
        Choose a trial multiplier λ_0^t = λ_0 + cDz_N.
        Find Π_k, R_k, λ_k^1, λ_k^2 using (13)–(17).
        Compute the error; Error^t = ‖z_N^t‖.
        Set c = c/10,  i = i + 1.
    end while
    Set λ_0 = λ_0^t, Error = Error^t. (accept the trial)
end while
```

Here i is the number of iterations, and $\epsilon_S, \alpha \in \mathbb{R}$ are stopping criterion and a scaling factor, respectively. The outer loop finds a search direction by computing the sensitivity derivatives, and the inner loop performs a line search to find the largest step size $c \in \mathbb{R}$ along the search direction. The error in satisfaction of the terminal boundary condition is determined at each inner iteration.

IV. Numerical Examples

Numerical optimization results for the 3D pendulum are given. Two elliptical cylinders, shown in Fig. 1, are used as rigid pendulum models. The properties are chosen as

Body (A): $m = 1,\ J = \mathrm{diag}[0.13, 0.28, 0.17], \rho = 0.3e_3.$

Body (B): $m = 1,\ J = \mathrm{diag}[0.22, 0.23, 0.03], \rho = 0.4e_3.$

Four cases are considered. Each maneuver is from a hanging equilibrium to another hanging equilibrium with a rotation about the vertical axis. The rotation angles are chosen as 90° and 180°. Since the vertical component of the angular momentum is set to zero, the rotation is purely caused by the geometric phase effect given in (3). These problems are challenging in the sense that the desired maneuvers are rotations about the gravity direction, but the control input cannot directly generate any moment about the gravity direction.

The corresponding boundary conditions are as follows.

(i) Body (A), hanging equilibrium to hanging equilibrium with 90° yaw

$$R_0 = I_{3\times 3}, \quad R_N^d = \begin{bmatrix} 0 & -1 & 0 \\ 1 & 0 & 0 \\ 0 & 0 & 1 \end{bmatrix},$$
$$\Pi_0 = 0_{3\times 1}, \quad \Pi_N^d = 0_{3\times 1}.$$

(ii) Body (A), hanging equilibrium to hanging equilibrium with 180° yaw

$$R_0 = I_{3\times 3}, \quad R_N^d = \mathrm{diag}[-1, -1, 1],$$
$$\Pi_0 = 0_{3\times 1}, \quad \Pi_N^d = 0_{3\times 1}.$$

(iii) Body (B), hanging equilibrium to hanging equilibrium with 90° yaw

$$R_0 = I_{3\times 3}, \quad R_N^d = \begin{bmatrix} 0 & -1 & 0 \\ 1 & 0 & 0 \\ 0 & 0 & 1 \end{bmatrix},$$
$$\Pi_0 = 0_{3\times 1}, \quad \Pi_N^d = 0_{3\times 1}.$$

(iv) Body (B), hanging equilibrium to hanging equilibrium with 180° yaw

$$R_0 = I_{3\times 3}, \quad R_N^d = \mathrm{diag}[-1, -1, 1],$$
$$\Pi_0 = 0_{3\times 1}, \quad \Pi_N^d = 0_{3\times 1}.$$

The optimal control results are given in Table I, where the optimized performance index, the error in satisfaction of the terminal boundary condition, and the simulation running time are shown for each case. The terminal error is at the level of machine precision, and the simulation time is about 5 minutes.

Figures 2–5 show snapshots of the attitude maneuvers, reduced trajectory of $\Gamma = R^T e_3$ on a sphere, control input history, and convergence rate. (A simple

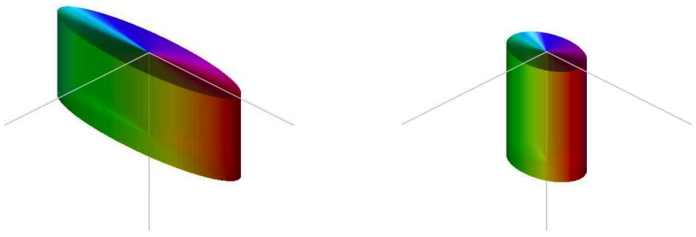

(a) Body (A) (b) Body (B)

Fig. 1. Elliptical cylinder

TABLE I

OPTIMIZATION RESULTS

Case	$\mathcal{J}$	$\left\|\log m(R_N^{d,T} R_N)\right\|$	$\left\|\Pi_N^d - \Pi_N\right\|$	ΔT
(i)	5.91	2.30×10^{-14}	1.34×10^{-14}	2.72
(ii)	7.32	4.80×10^{-15}	1.66×10^{-14}	5.25
(iii)	1.73	1.22×10^{-15}	6.55×10^{-14}	4.09
(iv)	3.37	3.06×10^{-14}	3.04×10^{-14}	5.05

ΔT: Simulation running time in Intel Pentium M 740 1.73GHz processor (min.)

animation for the attitude maneuver can be seen at `http://www.umich.edu/~tylee`.)

The convergence rate figures show violation of the terminal boundary condition according to the number of iterations in a logarithm scale. Red circles denote outer iterations in Newton-Armijo iteration to compute the sensitivity derivatives. For all cases, the initial guesses of the unspecified initial multiplier are arbitrarily chosen. The error in satisfaction of the terminal boundary condition converges quickly to machine precision after the solution is close to the local minimum at around 50th iteration. These convergence results are consistent with the quadratic convergence rates expected of Newton methods with accurately computed gradients. The condition number of the decomposed sensitivity derivative given at (21) varies from 10^0 to 10^5. If the sensitivity derivative is not decomposed, then the condition numbers are at the level of 10^{19}, and the numerical iterations fail.

The numerical examples presented in this paper show excellent numerical convergence properties. This is because the proposed computational algorithms on $\mathrm{SO}(3)$are geometrically exact and numerically accurate. In addition, the algorithm incorporates a modification that eliminates the singularity caused by the symmetry.

We interpret the optimization results using the geometric phase formula given by (3). For given initial conditions, the vertical component of the initial angular momentum is zero. Thus, the rotation about the vertical axis is purely caused by the geometric phase. Since the geometric phase is determined by a surface integral on $\mathbb{S}^2$ whose boundary is the reduced trajectory Γ, it is more efficient for the reduced trajectory to enclose the area at which the absolute value of the integrand of (3) is maximized.

In each subfigure (b) of Figures 2–5, the infinitesimal geometric phase per unit area is shown by color shading. The reduced trajectory, which represents the gravity direction in the body fixed frame, is shown by a solid line. The north pole of the sphere corresponds to the hanging equilibrium manifold, and the reduced trajectory starts and ends at the same north pole for the given boundary conditions.

Comparing Figures 2(b), 3(b) with Figure 4(b), 5(b), it can be seen that Body (A) and Body (B) have different geometric phase characteristics. This is caused by the fact that the geometric phase depends on the moment of inertia of the body. For Body (A), the absolute value of the infinitesimal geometric phase is maximized at a point on the equator, and for Body (B), it is maximized at the north pole. We see that the optimized reduced trajectories try to enclose those points.

As a result, the optimized attitude maneuver of Body (A) is distinguished from that of Body (B). The attitude maneuver of Body (A) is relatively more aggressive than that of Body (B) since the reduced trajectory passes near the equator corresponding to a horizontal position. Body (B) does not have to move far away from the hanging equilibrium since the infinitesimal geometric phase is maximized at that point. The resulting attitude maneuver is relatively benign.

REFERENCES

[1] E. Hairer, C. Lubich, and G. Wanner, *Geometric Numerical Integration*. Springer, 2002.

[2] T. Lee, M. Leok, and N. H. McClamroch, "A Lie group variational integrator for the attitude dynamics of a rigid body with applications to the 3D pendulum," in *Proceedings of the IEEE Conference on Control Applications*, 2005, pp. 962–967.

[3] ——, "Lie group variational integrators for the full body problem," *Computer Methods in Applied Mechanics and Engineering*, 2005, submitted. [Online]. Available: http://arxiv.org/math.NA/0508365

[4] K. Spindler, "Optimal control on Lie groups with applications to attitude control," *Mathematics of Control, Signals, and Systems*, vol. 11, pp. 197–219, 1998.

[5] S. Sastry, "Optimal control on Lie groups," in *Proceedings of the Third International Congress on Industrial and Applied Mathematics (ICIAM)*, 1995.

[6] V. Jurdjevic, *Geometric Control Theory*. Cambridge University, 1997.

[7] T. Lee, M. Leok, and N. H. McClamroch, "Optimal attitude control of a rigid body using geometrically exact computations on SO(3)," *Journal of Optimization Theory and Applications*, 2006, submitted. [Online]. Available: http://arxiv.org/math.OC/0601424

[8] ——, "Optimal control of a rigid body using geometrically exact computations on SE(3)," in *IEEE Conference on Decision and Control*, 2006, accepted. [Online]. Available: http://arxiv.org/math.OC/0602588

[9] J. Shen, A. K. Sanyal, N. A. Chaturvedi, D. Bernstein, and N. H. McClamroch, "Dynamics and control of a 3D pendulum," in *Proceedings of 43rd IEEE Conference on Decision and Control*, Dec. 2004, pp. 323–328.

[10] J. E. Marsden, R. Montgomery, and T. S. Ratiu, *Reduction, Symmetry and Phases in Mechanics*. American Mathematical Society, 1990.

[11] J. E. Marsden and M. West, "Discrete mechanics and variational integrators," *Acta Numerica*, vol. 10, pp. 357–514, 2001.

[12] A. Iserles, H. Z. Munthe-Kaas, S. P. Nørsett, and A. Zanna, "Lie-group methods," *Acta Numerica*, vol. 9, pp. 215–365, 2000.

[13] C. T. Kelley, *Iterative Methods for Linear and Nonlinear Equations*. SIAM, 1995.

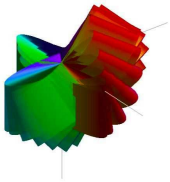

(a) Attitude Maneuver

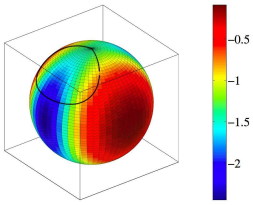

(b) Geometric Phase

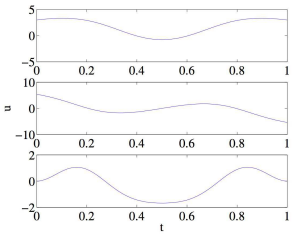

(c) Control Input

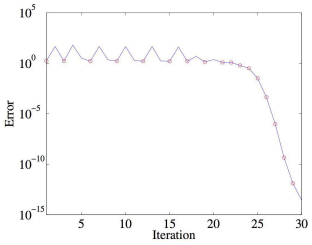

(d) Convergence Rate

Fig. 2. (i) Body A, hanging equilibrium to hanging equilibrium with 90° yaw

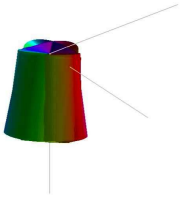

(a) Attitude Maneuver

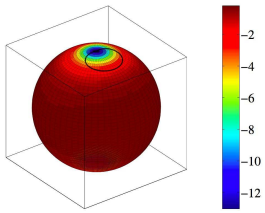

(b) Geometric Phase

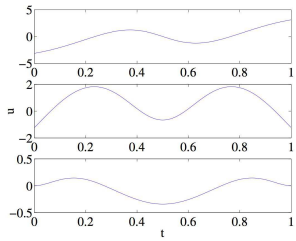

(c) Control Input

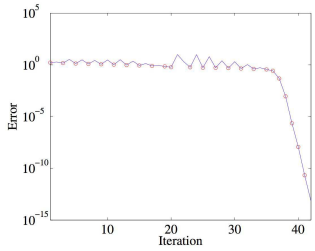

(d) Convergence Rate

Fig. 4. (iii). Body B, hanging equilibrium to hanging equilibrium with 90° yaw

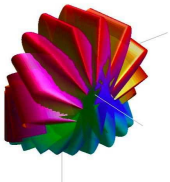

(a) Attitude Maneuver

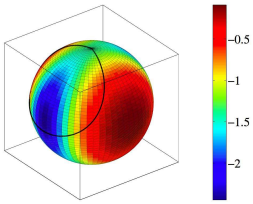

(b) Geometric Phase

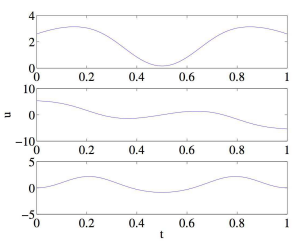

(c) Control Input

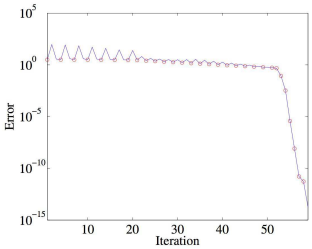

(d) Convergence Rate

Fig. 3. (ii). Body A, hanging equilibrium to hanging equilibrium with 180° yaw

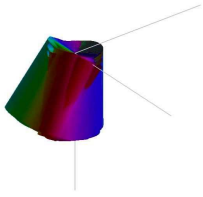

(a) Attitude Maneuver

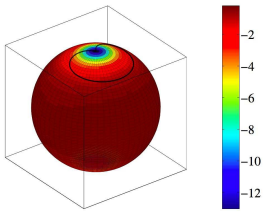

(b) Geometric Phase

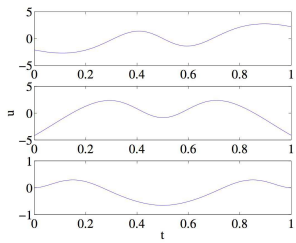

(c) Control Input

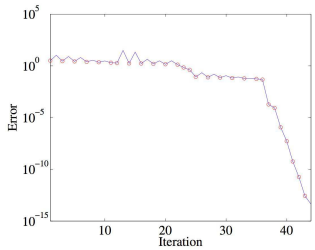

(d) Convergence Rate

Fig. 5. (iv). Body B, hanging equilibrium to hanging equilibrium with 180° yaw